JACS
JOURNAL OF THE AMERICAN CHEMICAL SOCIETY

ARTICLE

pubs.acs.org/JACS

Surfactant-Free Water-Processable Photoconductive All-Carbon Composite

Vincent C. Tung,[†] Jen-Hsien Huang,[†,‡] Ian Tevis,[§] Franklin Kim,[†] Jaemyung Kim,[†] Chih-Wei Chu,[†,‡] Samuel I. Stupp,[†,⊥,§] and Jiaxing Huang*[,†]

[†]Department of Materials Science and Engineering and [§]Department of Chemistry, Northwestern University, Evanston, Illinois 60208, United States

[‡]Research Center for Applied Sciences, Academia Sinica, Taipei, Taiwan 11529

[⊥]Feinberg School of Medicine, Northwestern University, Chicago, Illinois 60611, United States

Supporting Information

ABSTRACT: Heterojunctions between different graphitic nanostructures, including fullerenes, carbon nanotubes and graphene-based sheets, have attracted significant interest for light to electrical energy conversion. Because of their poor solubility, fabrication of such all-carbon nanocomposites typically involves covalently linking the individual constituents or the extensive surface functionalization to improve their solvent processability for mixing. However, such strategies often deteriorate or contaminate the functional carbon surfaces. Here we report that fullerenes, pristine single walled carbon nanotubes, and graphene oxide sheets can be conveniently coassembled in water to yield a stable colloidal dispersion for thin film processing. After thermal reduction of graphene oxide, a solvent-resistant photoconductive hybrid of fullerene−nanotube−graphene was obtained with on−off ratio of nearly 6 orders of magnitude. Photovoltaic devices made with the all-carbon hybrid as the active layer and an additional fullerene block layer showed unprecedented photovoltaic responses among all known all-carbon-based materials with an open circuit voltage of 0.59 V and a power conversion efficiency of 0.21%. The ease of making such surfactant-free, water-processed, carbon thin films could lead to their wide applications in organic optoelectronic devices.

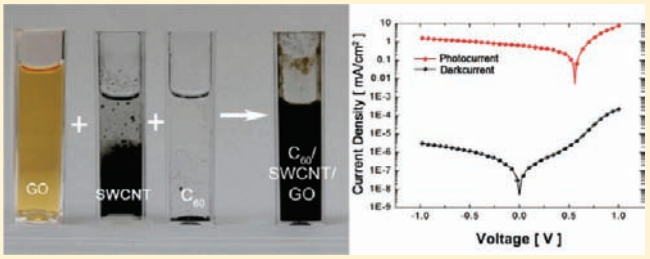

INTRODUCTION

Graphitic nanostructures are usually used as adducts to facilitate the separation, transport, and collection of photodissociated charges in organic optoelectronic devices.[1−8] Since fullerenes are n-type semiconductors,[9] while semiconducting carbon nanotubes[10,11] and graphene-based sheets[12,13] exhibit p-type-like behavior in ambient conditions, nanoscopic heterojunctions can be generated if these carbon nanostructures are brought together.[1−7,14] Because of their poor solubility, fabrication of such all-carbon nanocomposites typically involves covalently linking the individual constituents or the extensive surface functionalization to improve their solvent processability before direct mixing.[1−7] However, such strategies tend to break the conjugated carbon networks or contaminate their functional surfaces thus compromising the material's performance. Recently we discovered that graphene oxide (GO), the chemical exfoliation product of graphite, can act as a surfactant sheet to stabilize oil droplets in water and disperse graphite and carbon nanotubes in water.[15−17] One of the advantages of using GO as a dispersing agent for carbon materials is the ability to generate clean, electrically addressable carbon−carbon interfaces in the final composite because GO can be cleanly converted to chemical-modified graphene (also known as reduced GO, r-GO) without producing hard-to-remove byproducts.[18−20] Here we extend and build upon our previous dispersion work to create functional all-carbon hybrids made of fullerenes, single walled carbon nanotubes (SWCNTs), and graphene. It was found that although GO cannot disperse fullerene molecules in water, synergistic coassembly of fullerene, unfunctionalized SWCNTs, and GO in water readily yields a stable colloidal dispersion. This opens up new possibilities for making all-carbon composite materials without the need for any surface functionalization or dispersing agents for fullerenes and the hard-to-process carbon nanotubes. The fullerene−SWCNT−graphene hybrid was found to exhibit unprecedented photoconductive and photovoltaic properties when compared to the all-carbon or carbon-rich materials made by previous methods.

EXPERIMENTAL SECTION

Graphite powder (SP-1 grade) was purchased from Bay Carbon, Inc. Single wall carbon nanotubes (P2-SWCNTs) were purchased from Carbon Solutions, Inc. GO was synthesized by a modified Hummers' method[21] as reported elsewhere.[22] The dispersion was extensively

Received: November 18, 2010
Published: March 10, 2011

dx.doi.org/10.1021/ja1103734 | J. Am. Chem. Soc. 2011, 133, 4940–4947

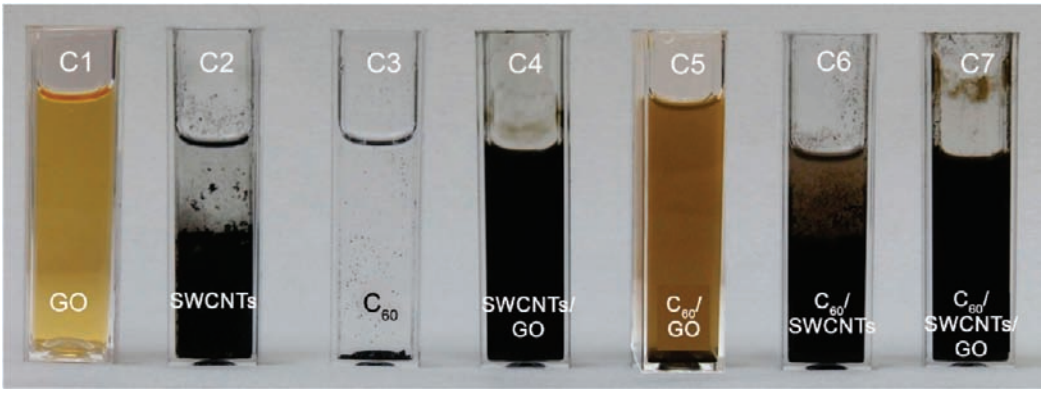

Figure 1. Picture of cuvettes C1−C7 containing aqueous dispersions of 1 mg/mL GO, 1 mg/mL SWCNTs, 0.5 mg/mL C_{60}, their binary blend SWCNTs/GO, C_{60}/GO, and C_{60}/SWCNTs, and the ternary blend C_{60}/SWCNTs/GO, respectively. The picture was taken 30 min after ultrasonication. GO can effectively disperse insoluble SWCNTs (C4) and C_{60}/SWCNTs complex (C7) in water, forming colloid dispersions that are stable for months.

washed and filtered to remove the salt byproduct and excess acid.[23] The dry GO filter cakes were redispersed in water to create a stock solution of 1 mg/mL, which may be further diluted to various concentrations. To create the dispersion of the binary mixtures of C_{60} (Nano C), unfunctionalized SWCNT powders, or GO, the individual components are blended in a mixture of water and methanol (10 to 1 volume ratio) and sonicated using a tip-sonicator (Misonix ultrasonic cell disruptors) for 2 h. Typically the concentrations of C_{60}, SWCNTs, and GO are 0.5, 1, and 1 mg/mL, respectively. To create the ternary composite, the three components were directly mixed and sonicated, or alternatively, C_{60} and SWCNT were first sonicated together to form a complex and then added into GO dispersion. Black colloidal dispersions with no visible precipitation were formed by either method. However, the dispersions made by the two-step mixing were found to produce more uniform thin films and therefore were used for preparing thin films for device studies. Typically to prepare the C_{60}/SWCNTs/GO hybrid, 100 μL of C_{60}/SWCNTs stock solution was carefully added into the GO solution (1 mg/mL) and was sonicated for two hour to ensure the stable colloidal dispersion. The resulting dispersion is stable for months.

Microscopy observations were made with scanning electron microscopy (SEM, Hitachi S-4800-II FEG), transmission electron microscopy (TEM, JEOL JEM-2100F), and atomic force microscopy (AFM, Multimode, DI). Confocal Raman spectroscopy studies were done at a fixed excitation wavelength of 514.5 nm on a silicon substrate. UV−vis spectra were acquired with an Agilent 8653 spectrometer. The spectra of SWCNTs and C_{60} were measured on the supernatant right after sonication. As for preparation of all-carbon composite devices, 5−8 nm thick active layer material of fullerene−SWCNTs−GO was spin coated onto a prepatterned indium tin oxide (ITO) anode (20 Ω/sq) with a thin buffer layer of poly(3,4-ethylenedioxythiophene):poly(styrenesulfonate) (PEDOT:PSS) (20 nm). The layer was annealed in ambient conditions at 150 °C for 30 min to reduce GO. A 15 nm thick corresponding fullerene layer was thermally evaporated followed by a 100 nm thick Al as the top electrode through a shadow mask. Photovoltaic measurements were done under AM1.5 80 mW cm^{-2} illumination from a Thermal Oriel Xe solar simulator equipped with an Oriel 130 monochromator. Filters were used to cut off grating overtones. A calibrated silicon reference solar cell with a KG5 filter certified by the National Renewable Energy Laboratory was used to confirm the measurement conditions. Device configurations for external quantum efficiency (EQE) measurement were similar to those used in photovoltaic measurement. The work function measurements were carried out by ultraviolet photoelectron spectroscopy (UPS) (ULVAC-PHI, Chigasaki) under ultrahigh-vacuum conditions (10^{-8} Pa). UPS spectra were collected on r-GO and SWCNTs thin films spin coated on the silver-coated silicon substrates under positive bias. Films were annealed at 150 °C in ambient conditions prior to characterization. Helium lamp emitting at 21.2 eV was used as the light source to excite the valence electrons.

RESULTS AND DISCUSSION

Synergistic Assembly of Fullerene, SWCNTs and GO. The cuvettes in Figure 1 contain the aqueous dispersions of GO, unfunctionalized SWCNTs, C_{60}, their binary mixtures, and the ternary mixture after ultrasonication treatment, respectively. As expected, GO (C1) disperses very well in water but SWCNTs (C2) and C_{60} (C3) do not. In an earlier work, we reported that GO can be used to disperse both multiwall and single wall carbon nanotubes in water through $\pi-\pi$ interaction.[16] The colloidal dispersion of SWCNT/GO (C4) was found to be stable for at least months and can be spin coated on a variety of substrates to create a smooth composite thin film (Figure 2a). However, attempts to disperse C_{60} powders with GO (C5) were not successful. After sonication, the majority of C_{60} powders remained in the precipitate. Although the supernatant did appear darker, SEM observation on spin-coated thin films revealed a large amount of micrometer- to submicrometer-sized particles covered by GO sheets (Figure 2b). Meanwhile, AFM measurements showed that the 1 nm apparent thicknesses of GO sheets before and after sonicating with C_{60} powder were largely unchanged (Figure 2b), suggesting that GO sheets were not coated by a C_{60} layer. Therefore the darkening of supernatant in C_{60}/GO dispersion (Figure 1, C5) is due to the formation of GO-stabilized C_{60} microcrystals during sonication. It has been known that C_{60} molecules can readily adsorb onto graphitic surfaces through strong van der Waals attraction.[24] However, since the basal plane of GO is functionalized with hydroxyl and epoxide groups, they effectively increase the separation between C_{60} and GO, thus screening off the van der Waals attraction.[25] As for SWCNTs or C_{60} microcrystals, they can adhere to GO sheets due to much larger interacting areas than individual C_{60} molecules. Although SWCNTs are insoluble in water, their graphitic nature can help to disperse C_{60} upon sonication, as evident by the much-reduced amount of powdery precipitates of C_{60} and much-darkened supernatant (Figure 1, C6). However, the C_{60}/SWCNT complex is not processable in water. Figure 2c shows that the

dx.doi.org/10.1021/ja1103734 |J. Am. Chem. Soc. 2011, 133, 4940–4947

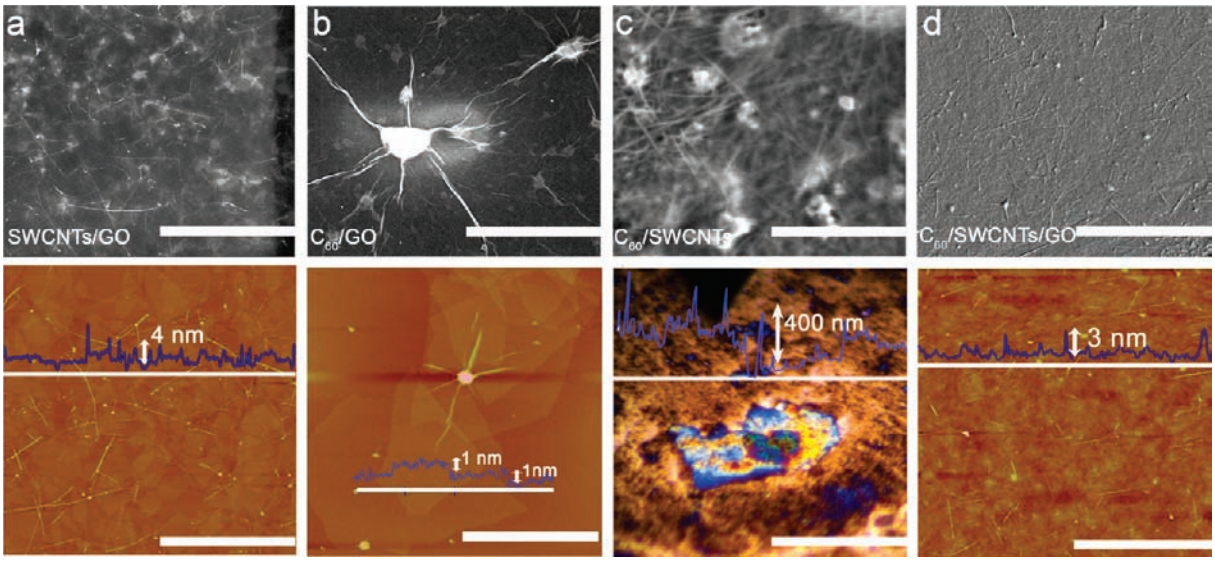

Figure 2. (Top): SEM images of spin-coated thin films of: (a) SWCNTs/GO; (b) C_{60}/GO; (c) C_{60}/SWCNTs; and (d) C_{60}/SWCNTs/GO, respectively. (Bottom): AFM (a, b, and d) and optical (c) images with height profile along the white line on each image. The optical image and height profile in (c) were obtained using a profilometer (Veeco Dektak 150). Scale bars = 2.5 μm.

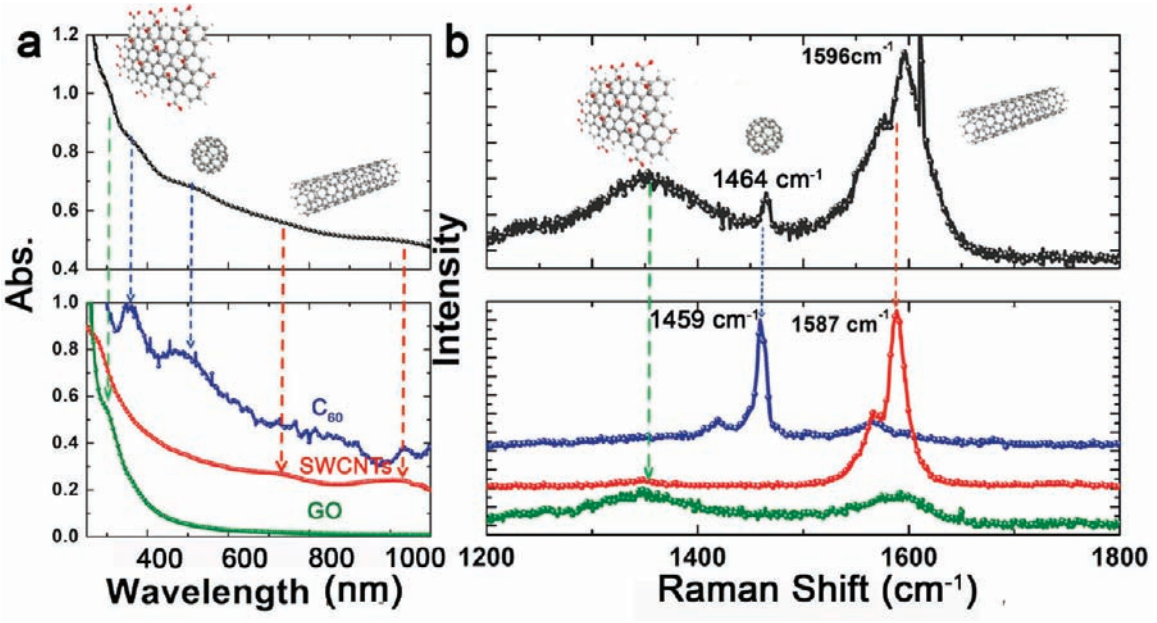

Figure 3. (a) Solution phase UV−vis and (b) solid-state Raman spectra (excitation wavelength of 514 nm) of the C_{60}/SWCNTs/GO composite and the individual components. Both spectra of the composite display a red shift, and the bands of the individual components were red shifted, suggesting strong $\pi-\pi$ stacking between the components.

spin-coated C_{60}/SWCNT thin film was very uneven with surface roughness at submicrometer scale.

If the basal plane of GO can be made more graphitic, it should become a better dispersing agent for C_{60} molecules. A straightforward idea would be reducing it to chemically modified graphene (r-GO). Unfortunately, the colloidal stability of r-GO sheets is much lower compared to GO,[26] making it less ideal for this purpose. Note that while GO makes SWCNTs water dispersible, the SWCNTs attached to the GO also effectively make the basal plane of GO sheets more graphitic. Therefore, a SWCNTs/GO complex should better disperse C_{60} molecules than GO. Indeed, colloidal dispersions of C_{60}/SWCNTs/GO can be successfully created by sonicating SWCNTs and C_{60} in GO water (Figure 1, C7). It can also be made by first creating C_{60}/SWCNTs (Figure 1, C6) and then dispersing the insoluble complex with GO. The dispersion can produce smooth thin films by spin coating (Figure 2d). Adding a small amount of methanol (up to 10 vol %) can greatly facilitate the dispersion due to improved wetting on the hydrophobic carbon surfaces as well as its deposition on common glass or silicon substrates. UV−vis spectrum (Figure 3a) of the ternary hybrid, C_{60}/SWCNTs/GO shows two bands characteristic of SWCNTs at around 750 and

dx.doi.org/10.1021/ja1103734 |J. Am. Chem. Soc. 2011, 133, 4940–4947

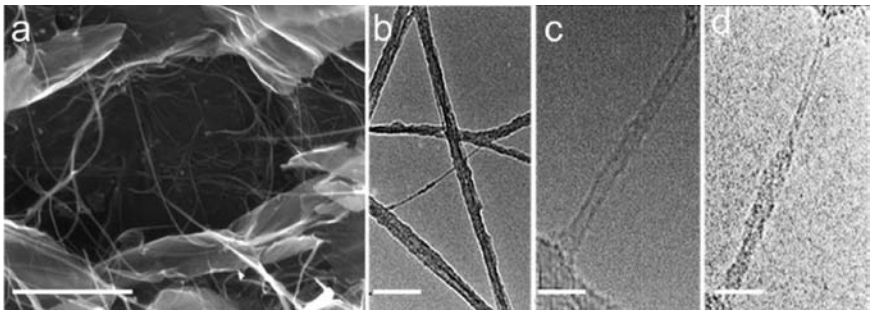

Figure 4. (a) High-magnification cross-sectional SEM image of a thick composite film clearly shows SWCNTs bridging the exfoliated graphene sheets. Scale bar = 500 nm. (b) Low-resolution TEM image of the C_{60}/SWCNTs reveals rough coatings on the SWCNTs. Scale bar = 50 nm. High-resolution TEM images of (c) a bare pristine SWCNT and (d) a SWCNT half coated with clusters of 1−2 nm after sonicating with C_{60} powders in water. Scale bars = 5 nm.

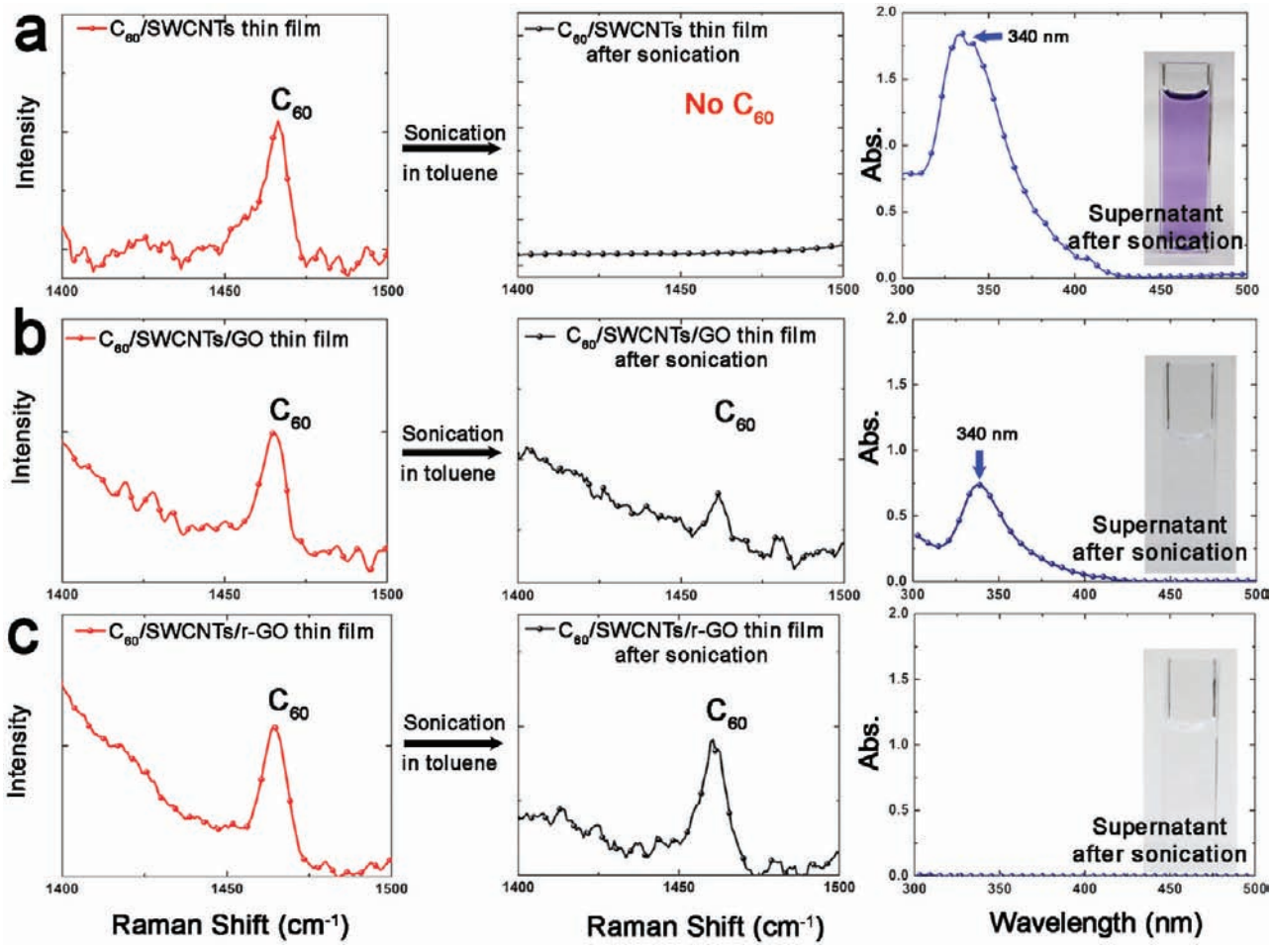

Figure 5. Thermal annealing of C_{60}/SWCNTs/GO creates a solvent-resistant all-carbon composite. Raman and UV−vis spectroscopy were used to monitor the amounts of C_{60} left in the solid samples of (a) C_{60}/SWCNTs, (b) C_{60}/SWCNTs/GO, and (c) C_{60}/SWCNTs/r-GO and in those released into toluene after sonication, respectively. The insets show the color of the supernatants. Results clearly show that GO and r-GO suppress the release of C_{60} into the supernatant.

930 nm (red, dashed arrows), respectively.[27] In addition, two distinct absorption bands at around 360 and 505 nm can be attributed to C_{60} (blue, dashed arrows).[28] Another band near 300 nm can be attributed to GO.[26] While the hybrid dispersion exhibits the characteristic absorption bands of each component, the overall spectrum was red shifted in regard to the individual constituents. This indicates intimate contact between these carbon nanomaterials formed by strong $\pi-\pi$ stacking. The ternary colloidal dispersions can be readily used for spin coating to make thin films. The Raman spectrum (Figure 3b) of the dried composite thin film shows signatures of all the constituents:[29] a stretching mode of C_{60} cages at 1464 cm^{-1}, two dominant peaks

dx.doi.org/10.1021/ja1103734 |*J. Am. Chem. Soc.* 2011, 133, 4940–4947

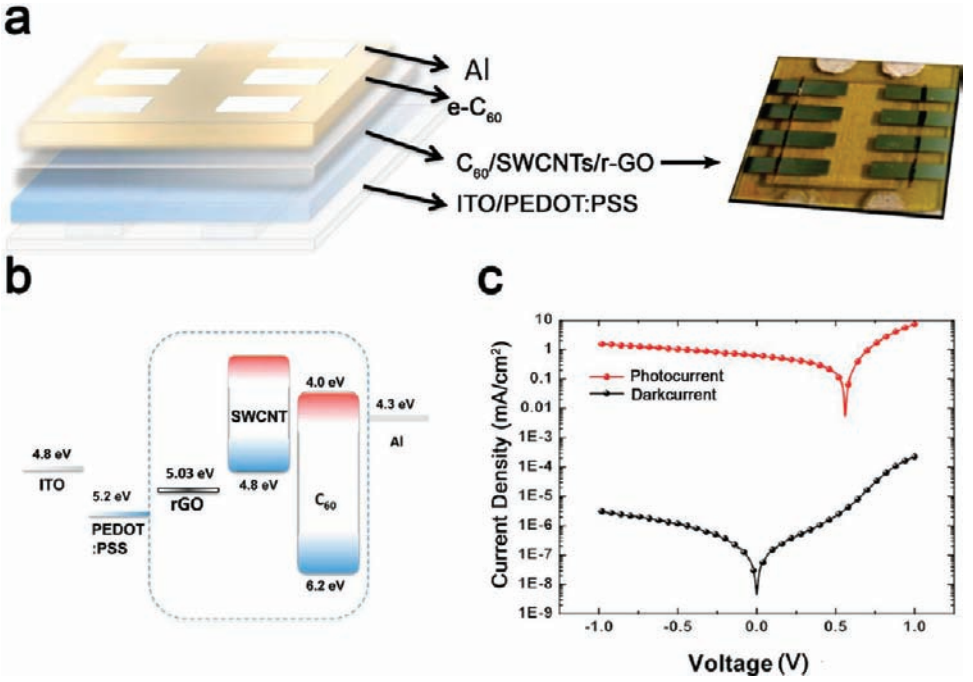

Figure 6. All-carbon photovoltaic device. (a) Schematic diagram illustrating the photovoltaic device structure with C_{60}/SWCNTs/r-GO as the active layer and an additional layer of thermally evaporated C_{60} as the protection/hole blocking layer. The photograph on the right shows one such device. (b) Corresponding schematic energy level diagram of the device. The all-carbon composite is shown in the dashed box. The IP of the SWCNTs sample is experimentally determined from a thin film comprised of a mixture of semiconducting and metallic nanotubes. LUMOs of SWCNTs is not marked because their band gap varies by diameter. (c) Representative $I-V$ curves measured in the dark and under illumination.

at 1596 and 1587 cm^{-1} associated with the phonon transition within the SWCNTs, and a D peak at 1350 cm^{-1} from GO. Note that the absence of a D band in the Raman spectrum of SWCNTs confirmed that their surfaces are unfunctionalized.

Solvent-Resistant All-Carbon Composite. After thermal treatment, the GO sheets in the film can be converted to chemically modified graphene, making the product a C_{60}/SWCNTs/r-GO all-carbon composite. Figure 4a is a cross-sectional SEM image of a thick film of such an all-carbon composite, which was thermally exfoliated to show SWCNTs bridging the r-GO sheets. TEM (Figure 4b) observation showed that the SWCNTs were largely debundled. Only individual tubes or bundles of a few tubes were found. High-resolution TEM images revealed that all the tubes have a rough coating on the surface. From half-coated tubes, the thickness of the coating was estimated to be around 1−2 nm thick, which is presumably a layer of C_{60} clusters (Figure 4c and d).[2]

The C_{60}/SWCNTs complexes (Figure 1, C6) formed by sonicating individual components in water can be readily dissociated in organic solvents that can dissolve fullerenes, such as toluene. However, the addition of GO not only helps to disperse the C_{60}/SWCNTs complex in water but also greatly improves the solvent resistivity of the complex as demonstrated by "toluene wash" tests on the composite thin films. Three thin films consisting of C_{60}/SWCNTs, C_{60}/SWCNTs/GO, and C_{60}/SWCNTs/r-GO were prepared. The samples were then sonicated in toluene for 10 min and thoroughly rinsed with toluene before dried in air. Raman and UV−vis spectroscopy were used to monitor the amounts of C_{60} left in the samples and released into toluene during sonication, respectively. In Figure 5a, Raman spectrum shows that C_{60} was completely removed from the C_{60}/SWCNTs complex. Meanwhile, the supernatant became purple with a nearly saturated, characteristic C_{60} absorption band at 340 nm in its UV−vis spectrum. For the C_{60}/SWCNTs/GO complex, dissociation of C_{60} was greatly suppressed (Figure 5b). This is likely due to the wrapping or sandwiching of C_{60}/SWCNTs complex, which is consistent with the thin film morphology revealed by SEM and AFM images (Figure 2d). After reducing GO, even tighter protection can be expected due to much increased $\pi-\pi$ and van der Waals attraction between C_{60}-coated SWCNTs and r-GO. Indeed, Raman and UV−vis spectra (Figure 5c) show that the solid thin film of C_{60}/SWCNTs/r-GO has become resistant to toluene even after sonication. Thus a clean, solvent-resistant, all-carbon composite made of C_{60}, SWCNTs, and graphene had been successfully created. The drastic change in solvent processability of such all-carbon composites before and after reduction opens up their use in solution-processed organic thin film devices, in which a great challenge is the materials' solvent stability during multilayer deposition.[30]

Photoconductive All-Carbon Composite and Photovoltaic Devices. Thin films of spin-coated C_{60}/SWCNTs/GO were found to exhibit surface roughness of around only a few nanometers (Figure 2d), which makes it possible to use them in photovoltaic devices. First, a C_{60}/SWCNTs/GO thin film of 5−8 nm was spin cast onto an ITO glass substrate, which was pretreated with a smooth 20 nm layer of PEDOT:PSS (Sigma-Aldrich). Thermal reduction of GO at 150 °C was found to turn the insulating composite sufficiently conductive. Next, an additional layer of 15 nm thick C_{60} was thermally evaporated onto the all-carbon active layer, acting both as a blocking layer to prevent shorting and as an electron-transporting layer. Finally, 100 nm thick of Al electrodes were deposited to complete the device.

Figure 6a shows the device structure using the C_{60}/SWCNTs/r-GO composite as the active layer. Corresponding schematic

dx.doi.org/10.1021/ja1103734 |J. Am. Chem. Soc. 2011, 133, 4940–4947

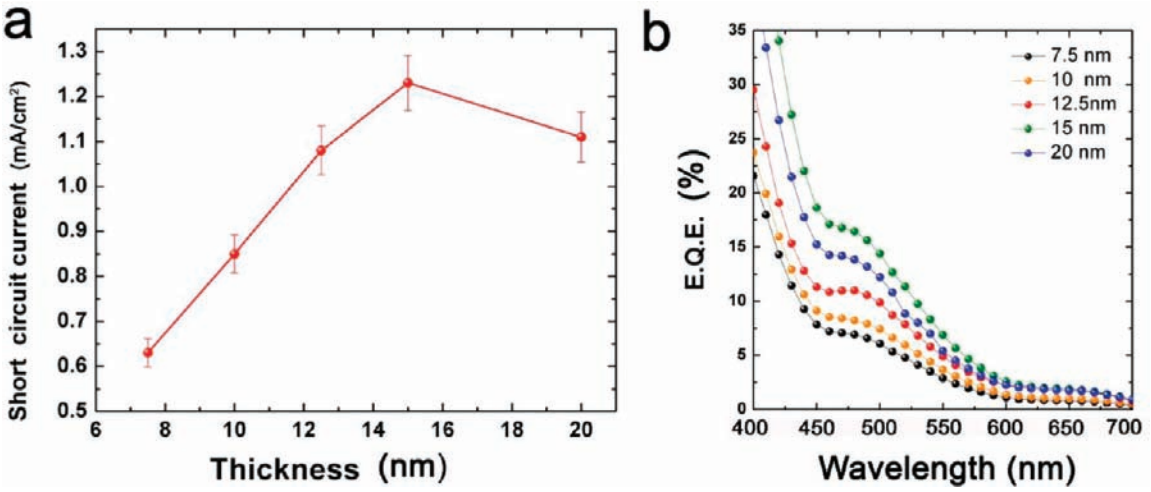

Figure 7. Effects of the thickness of the thermally evaporated C_{60} blocking layer (e-C_{60}) on (a) the short circuit current and (b) corresponding EQE of the devices. The optimal thickness was found to be around 15 nm.

diagram of the energy levels of the individual components is shown in Figure 6b. The work functions of ITO, PEDOT:PSS, and Al, the energy level of the highest occupied molecular orbital (HOMO) and the lowest unoccupied molecular orbital (LUMO)[14,31,32] of C_{60}, are taken from literature. The ionization potentials (IP) of r-GO and SWCNTs were determined by ultraviolet photoelectron spectroscopy (UPS) to be 5.0 and 4.8 eV, respectively (Supporting Information, Figure S1). Since the SWCNTs sample used here (Carbon Solution Inc. P2-SWCNT) was made by arc-discharge method, which contains both metallic and semiconducting nanotubes of various chiralities,[33,34] the measured IP of the SWCNTs sample could correspond to the work function of the metallic nanotubes or the HOMO level of the semiconducting ones. Since a random distribution of chirality would result in one-third of metallic and two-thirds of semiconducting nanotubes,[35] we assume there were more semiconducting nanotubes in the sample. Therefore, the IP was taken to represent the average HOMO level of the semiconducting carbon nanotubes in the sample. The LUMO value is not marked on the diagram (Figure 6b) since the band gap of semiconducting carbon nanotubes varies by diameter, which is polydispersed in the sample. The energy level offset at the C_{60}/SWCNTs heterojunction is sufficiently large to dissociate photogenerated excitons. Electrons and holes can then be transported to the corresponding electrodes through the e-C_{60} and SWCNTs/r-GO network, respectively, to generate photocurrent. The output current−voltage characteristics of the device are shown in Figure 6c. The dark current exhibits a distinct diode behavior with a rectification ratio of 10^4. Upon illumination (AM 1.5, 80 mW/cm^2), the device showed a photoconductive response with an on/off ratio of near 10^6, which surpasses those of covalently linked, polymer-wrapped, or extensively surface functionalized all-carbon composites.[1,4−6] More significantly, the device displayed an unprecedented photovoltaic response for devices using all-carbon-based materials as the active layer,[1−7] with a short circuit current (J_{sc}) of 1.23 mA/cm^2, an open circuit voltage (V_{oc}) of 0.59 V, and a fill factor of 0.29, giving rise to a power conversion efficiency of 0.21%.

Figure 7 shows the effects of the thickness of the evaporated C_{60} layer on the device's photocurrent and external quantum efficiency (EQE). Typically an e-C_{60} layer is used to assist electron transport, retard hole transport, and prevent shorting. The optimal thickness was found to be around 15 nm yielding a PCE of 0.21%. When the thickness of this layer was increased from 7.5, 10, 12.5, to 15 nm, gradual increase in photocurrent was observed. The same trend is observed in EQE measurement, suggesting that the e-C_{60} layer is also contributing to light absorption, in addition to being the electron-transporting and hole-blocking layer. However, decreased photocurrent and EQE were observed when the thickness of e-C_{60} exceeded 20 nm. This is attributed to increased probability of charge recombination due to short exciton diffusion length, which limited the overall production of photocurrent.

Although this e-C_{60} layer is also contributing the light absorption, devices using only the evaporated C_{60} thin film (e-C_{60}, 15 nm thick) as the active layer lacked effective means for hole transport, yielding a photocurrent 3 orders of magnitude lower than those using the all-carbon composite (Figure 8, green line). Since C_{60}, SWCNTs, C_{60}/SWCNTs, or C_{60}/GO were not processable (Figure 1), their spin-coated thin films were very rough and uneven (Figure 2). As a result, all these devices failed due to shorting. Smooth films of SWCNTs/GO were obtained, and the corresponding SWCNTs/r-GO devices did produce a photovoltaic effect since there are also heterojunctions between the e-C_{60} and SWCNTs (Figure 8, red line). However, the photocurrent of the ternary all-carbon composite was 2 orders of magnitude higher (Figure 8, black line) likely due to the preassembled C_{60} helping to form higher quality interfaces and heterojunctions between SWCNTs and the evaporated C_{60}.

These control experiments suggest that in the all-carbon composite, GO's main function is in material processing. It acts as a dispersing agent to enable solution processability of C_{60}/SWCNTs. In addition, its sheet-like morphology helps to lower the surface roughness of the spin-coated thin films, which is critical for making photovoltaic devices. The insulating GO can be "cured" by gentle heating to become conductive and insoluble, thus electrically activating the device and preventing C_{60} from leaching out of the composite. The efficiency of the all-carbon composite devices here should be readily improved by optimizing the relative fractions of the individual constituents to obtain processable ternary composites with maximal content of C_{60}/SWCNTs heterojunctions. Other possible means include reducing the size of GO sheets,[36] optimizing the reduction conditions for

dx.doi.org/10.1021/ja1103734 |J. Am. Chem. Soc. 2011, 133, 4940–4947

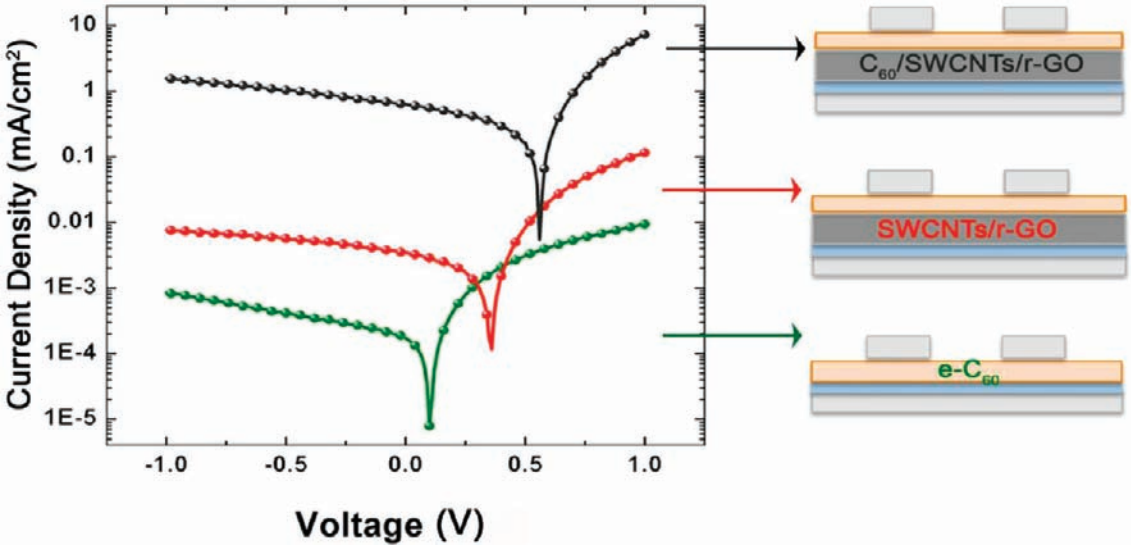

Figure 8. Control devices made with only e-C_{60} (15 nm, green line) or SWCNTs/r-GO + e-C_{60} (red line) produced orders of magnitude lower photocurrent and decreased V_{oc} compared to the all-carbon hybrid device (black line).

GO, removing the metallic nanotubes from the SWCNTs sample, and/or using a more efficient light absorbing fullerenes, such as C_{70}. These will also help to better understand the role of each carbon building blocks in the device.

CONCLUSION

In conclusion, surfactant-free, water-processable composites made of C_{60}, SWCNTs, and GO can be conveniently created by simply assembling the constituents in water. Gentle thermal treatment turns it into a solvent-resistant, photoconductive all-carbon composite, which displays unprecedented photoconductive responses with an on/off ratio of nearly 10^6 and a photovoltaic effect with a V_{oc} of 0.59 V and a power conversion efficiency of 0.21%. With the great variety of different fullerenes, carbon nanotubes, and graphene derivatives, numerous types of all-carbon composites can be envisioned through this "green" processing route that could lead to exciting new materials for energy conversion and storage. The coassembly strategy to create all-carbon composite reported here should be applicable to prepare many other water-based, carbon-rich photovoltaic materials by dispersing hard-to-process aromatic dyes on SWCNTs/GO scaffolds.

ASSOCIATED CONTENT

Supporting Information. UPS spectra of P2-SWCNTs and r-GO thin film casted on silver-coated silicon substrates. This material is available free of charge via the Internet at http://pubs.acs.org.

AUTHOR INFORMATION

Corresponding Author
jiaxing-huang@northwestern.edu

ACKNOWLEDGMENT

This work was supported by a booster award from the Initiative for Sustainability and Energy at Northwestern University (ISEN) and the National Science Foundation through a CAREER award (DMR 0955612). Additional support was provided by the Sony Corporation and the Northrop Grumman Corporation. C—W.C. is grateful to the National Science Council (NSC), Taiwan (99-2221-E-001-012) and the Academia Sinica research program on nanoscience and nanotechnology for financial support. S.I.S acknowledges support from the U.S. Department of Energy, Office of Basic Energy Sciences (DE-FG02-00ER45810). The authors would also like to thank L.J. Cote, J. Luo, K. Sohn, T.H. Han, W. W. Tsai, and A.R. Koltonow for lending their expertise and helpful discussions. We thank the NUANCE Center, which is supported by NSF-NSEC, NSF-MRSEC, Keck Foundation, the State of Illinois, and Northwestern University for use of their microscopy and surface analysis facilities.

REFERENCES

(1) Yamamoto, Y.; Fukushima, T.; Suna, Y.; Ishii, N.; Saeki, A.; Seki, S.; Tagawa, S.; Taniguchi, M.; Kawai, T.; Aida, T. *Science* **2006**, *314*, 1761–1764.
(2) Nasibulin, A. G.; et al. *Nat. Nanotechnol.* **2007**, *2*, 156–161.
(3) Umeyama, T.; Tezuka, N.; Fujita, M.; Hayashi, S.; Kadota, N.; Matano, Y.; Imahori, H. *Chem.—Eur. J.* **2008**, *14*, 4875–4885.
(4) Kalita, G.; Adhikari, S.; Aryal, H. R.; Umeno, M.; Afre, R.; Soga, T.; Sharon, M. *Appl. Phys. Lett.* **2008**, *92*, No. 123508.
(5) Yamamoto, Y.; Zhang, G. X.; Jin, W. S.; Fukushima, T.; Ishii, N.; Saeki, A.; Seki, S.; Tagawa, S.; Minari, T.; Tsukagoshi, K.; Aida, T. *Proc. Natl. Acad. Sci. U.S.A.* **2009**, *106*, 21051–21056.
(6) Umeyama, T.; Tezuka, N.; Seki, S.; Matano, Y.; Nishi, M.; Hirao, K.; Lehtivuori, H.; Tkachenko, N. V.; Lemmetyinen, H.; Nakao, Y.; Sakaki, S.; Imahori, H. *Adv. Mater.* **2010**, *22*, 1767–1770.
(7) Zhang, X. Y.; Huang, Y.; Wang, Y.; Ma, Y. F.; Liu, Z. F.; Chen, Y. S. *Carbon* **2009**, *47*, 334–337.
(8) Zhu, H. W.; Wei, J. Q.; Wang, K. L.; Wu, D. H. *Sol. Energy Mater.* **2009**, *93*, 1461–1470.
(9) Sariciftci, N. S.; Smilowitz, L.; Heeger, A. J.; Wudl, F. *Science* **1992**, *258*, 1474–1476.
(10) Tans, S. J.; Verschueren, A. R. M.; Dekker, C. *Nature* **1998**, *393*, 49–52.
(11) Durkop, T.; Getty, S. A.; Cobas, E.; Fuhrer, M. S. *Nano Lett.* **2004**, *4*, 35–39.

(12) Gilje, S.; Han, S.; Wang, M.; Wang, K. L.; Kaner, R. B. *Nano Lett.* **2007**, *7*, 3394–3398.
(13) Eda, G.; Fanchini, G.; Chhowalla, M. *Nat. Nanotechnol.* **2008**, *3*, 270–274.
(14) Arnold, M. S.; Zimmerman, J. D.; Renshaw, C. K.; Xu, X.; Lunt, R. R.; Austin, C. M.; Forrest, S. R. *Nano Lett.* **2009**, *9*, 3354–3358.
(15) Kim, F.; Cote, L. J.; Huang, J. X. *Adv. Mater.* **2010**, *22*, 1954–1958.
(16) Kim, J.; Cote, L. J.; Kim, F.; Yuan, W.; Shull, K. R.; Huang, J. X. *J. Am. Chem. Soc.* **2010**, *132*, 8180–8186.
(17) Cote, L. J.; Kim, J.; Tung, V. C.; Luo, J.; Kim, F.; Huang, J. X. *Pure Appl. Chem.* **2011**, *83*, 95–110.
(18) Schniepp, H. C.; Li, J. L.; McAllister, M. J.; Sai, H.; Herrera-Alonso, M.; Adamson, D. H.; Prud'homme, R. K.; Car, R.; Saville, D. A.; Aksay, I. A. *J. Phys. Chem. B* **2006**, *110*, 8535–8539.
(19) Stankovich, S.; Dikin, D. A.; Dommett, G. H. B.; Kohlhaas, K. M.; Zimney, E. J.; Stach, E. A.; Piner, R. D.; Nguyen, S. T.; Ruoff, R. S. *Nature* **2006**, *442*, 282–286.
(20) Cote, L. J.; Cruz-Silva, R.; Huang, J. X. *J. Am. Chem. Soc.* **2009**, *131*, 11027–11032.
(21) Hummers, W. S.; Offeman, R. E. *J. Am. Chem. Soc.* **1958**, *80*, 1339–1339.
(22) Cote, L. J.; Kim, F.; Huang, J. X. *J. Am. Chem. Soc.* **2009**, *131*, 1043–1049.
(23) Kim, F.; Luo, J.; Cruz-Silva, R.; Cote, L. C.; Sohn, K.; Huang, J. *Adv. Funct. Mater.* **2010**, *20*, 2867–2873.
(24) Ruoff, R. S.; Hickman, A. P. *J. Phys. Chem.* **1993**, *97*, 2494–2496.
(25) Israelachvili, J. N. *Intermolecular and Surface Forces*; 2nd ed.; Academic Press: Burlington, MA, 1992.
(26) Li, D.; Muller, M. B.; Gilje, S.; Kaner, R. B.; Wallace, G. G. *Nat. Nanotechnol.* **2008**, *3*, 101–105.
(27) Ausman, K. D.; Piner, R.; Lourie, O.; Ruoff, R. S.; Korobov, M. *J. Phys. Chem. B* **2000**, *104*, 8911–8915.
(28) Hare, J. P.; Kroto, H. W.; Taylor, R. *Chem. Phys. Lett.* **1991**, *177*, 394–398.
(29) Dresselhaus, M. S.; Jorio, A.; Hofmann, M.; Dresselhaus, G.; Saito, R. *Nano Lett.* **2010**, *10*, 751–758.
(30) Hagemann, O.; Bjerring, M.; Nielsen, N. C.; Krebs, F. C. *Sol. Energy Mater.* **2008**, *92*, 1327–1335.
(31) Sato, N.; Saito, Y.; Shinohara, H. *Chem. Phys.* **1992**, *162*, 433–438.
(32) Shirley, E. L.; Louie, S. G. *Phys. Rev. Lett.* **1993**, *71*, 133–136.
(33) Journet, C.; Maser, W. K.; Bernier, P.; Loiseau, A.; delaChapelle, M. L.; Lefrant, S.; Deniard, P.; Lee, R.; Fischer, J. E. *Nature* **1997**, *388*, 756–758.
(34) Henrard, L.; Loiseau, A.; Journet, C.; Bernier, P. *Synth. Met.* **1999**, *103*, 2533–2536.
(35) Wildoer, J. W. G.; Venema, L. C.; Rinzler, A. G.; Smalley, R. E.; Dekker, C. *Nature* **1998**, *391*, 59–62.
(36) Luo, J.; Cote, L. J.; Tung, V. C.; Tan, A. T. L.; Goins, P. E.; Wu, J.; Huang, J. X. *J. Am. Chem. Soc.* **2010**, *132*, 17667–17669.